



In vivo dynamics of acidosis and oxidative stress in the acute phase of an ischemic stroke in a rodent model

Ilya V. Kelmanson^{a,b,1}, Arina G. Shokhina^{a,b,1}, Daria A. Kotova^{a,1}, Matvei S. Pochechuev^c, Alexandra D. Ivanova^{a,d}, Alexander I. Kostyuk^a, Anastasiya S. Panova^a, Anastasia A. Borodinova^e, Maxim A. Solotnikov^c, Evgeny A. Stepanov^{c,f}, Roman I. Raevskii^a, Aleksandr A. Moshchenko^g, Valeriy V. Pak^{a,2}, Yulia G. Ermakova^{h,3}, Gijsbert J.C. van Belleⁱ, Viktor Tarabykin^j, Pavel M. Balaban^e, Ilya V. Fedotov^{c,f,k,1}, Andrei B. Fedotov^{c,f}, Marcus Conrad^{b,m}, Ivan Bogeskiⁱ, Dörthe M. Katschinskiⁱ, Thorsten R. Doeppner^{n,o,p}, Mathias Bährⁿ, Aleksei M. Zheltikov^{c,f,k,1}, Dmitry S. Bilan^{a,b,*}, Vsevolod V. Belousov^{a,b,g,i,**}

^a M.M. Shemyakin and Yu.A. Ovchinnikov Institute of Bioorganic Chemistry, Russian Academy of Sciences, Moscow, 117997, Russia

^b Laboratory of Experimental Oncology, Pirogov Russian National Research Medical University, 117997, Moscow, Russia

^c Physics Department, International Laser Center, M.V. Lomonosov Moscow State University, Moscow, 119992, Russia

^d Biological Department, M.V. Lomonosov Moscow State University, Moscow, 119992, Russia

^e Institute of Higher Nervous Activity and Neurophysiology, Russian Academy of Sciences, Moscow, 117485, Russia

^f Russian Quantum Center, Skolkovo, Moscow Region, 143025, Russia

^g Federal Center of Brain Research and Neurotechnologies, Federal Medical Biological Agency, Moscow, 117997, Russia

^h European Molecular Biology Laboratory, Heidelberg, 69117, Germany

ⁱ Institute for Cardiovascular Physiology, University Medical Center Göttingen, Georg-August-University, Humboldtallee 23, 37073, Göttingen, Germany

^j Institute of Cell Biology and Neurobiology, Charité - Universitätsmedizin Berlin, Berlin, 10117, Germany

^k Kazan Quantum Center, A.N. Tupolev Kazan National Research Technical University, Kazan, 420126, Russia

^l Department of Physics and Astronomy, Texas A&M University, College Station, TX, 77843, USA

^m Helmholtz Zentrum München, Institute of Metabolism and Cell Death, Ingolstädter Landstr. 1, Neuherberg, 85764, Germany

ⁿ Department of Neurology, University Medical Center Göttingen, Göttingen, 37075, Germany

^o Istanbul Medipol University, Research Institute for Health Sciences and Technologies (SABITA), Istanbul, Turkey

^p Istanbul Medipol University, School of Medicine, Dept. of Physiology, Istanbul, Turkey

ARTICLE INFO

Keywords:

Ischemic stroke
Ischemia/reperfusion
Hypoxia/reoxygenation
In vivo optical brain interrogation
Genetically encoded fluorescent biosensors
Hydrogen peroxide

ABSTRACT

Ischemic cerebral stroke is one of the leading causes of death and disability in humans. However, molecular processes underlying the development of this pathology remain poorly understood. There are major gaps in our understanding of metabolic changes that occur in the brain tissue during the early stages of ischemia and reperfusion. In particular, it is generally accepted that both ischemia (I) and reperfusion (R) generate reactive oxygen species (ROS) that cause oxidative stress which is one of the main drivers of the pathology, although ROS generation during I/R was never demonstrated *in vivo* due to the lack of suitable methods. In the present study, we record for the first time the dynamics of intracellular pH and H₂O₂ during I/R in cultured neurons and during experimental stroke in rats using the latest generation of genetically encoded biosensors SypHer3s and HyPer7. We detect a buildup of powerful acidosis in the brain tissue that overlaps with the ischemic core from the first seconds of pathogenesis. At the same time, no significant H₂O₂ generation was found in the acute phase of

Abbreviations: AAV, adeno-associated virus; cpYFP, circularly permuted yellow fluorescent protein; I/R, ischemia/reperfusion; MCAO, Middle Cerebral Artery Occlusion; NAD, nicotinamide adenine dinucleotide: NADH (reduced) and NAD⁺ (oxidized); NADPH, nicotinamide adenine dinucleotide phosphate; NOX, NADPH-oxidase; ROS, reactive oxygen species; SHR, spontaneously hypertensive rat; TTC, 2,3,5-triphenyltetrazolium chloride.

* Corresponding author. M.M. Shemyakin and Yu.A. Ovchinnikov Institute of Bioorganic Chemistry, Russian Academy of Sciences, Moscow, 117997, Russia.

** Corresponding author. Federal Center of Brain Research and Neurotechnologies, Federal Medical Biological Agency, Moscow, 117997, Russia.

E-mail addresses: d.s.bilan@gmail.com (D.S. Bilan), belousov@fccps.ru (V.V. Belousov).

¹ These authors contributed equally.

² Present address: European Molecular Biology Laboratory, Heidelberg 69117, Germany

³ Present address: European Molecular Biology Laboratory Rome, Monterotondo (RM) 00015, Italy

<https://doi.org/10.1016/j.redox.2021.102178>

Received 9 October 2021; Received in revised form 1 November 2021; Accepted 2 November 2021

Available online 3 November 2021

2213-2317/© 2021 Published by Elsevier B.V. This is an open access article under the CC BY-NC-ND license (<http://creativecommons.org/licenses/by-nc-nd/4.0/>).

ischemia/reperfusion. HyPer7 oxidation in the brain was detected only 24 h later. Comparison of *in vivo* experiments with studies on cultured neurons under I/R demonstrates that the dynamics of metabolic processes in these models significantly differ, suggesting that a cell culture is a poor predictor of metabolic events *in vivo*.

1. Introduction

Oxygen plays a key role in the metabolism of aerobic organisms, serving, primarily, to maintain the energy cellular balance. The mammalian brain is the most energy-consuming organ [1]. Thus, even a short termination of oxygen supply causes significant metabolic changes in brain tissue, which leads to irreversible consequences in a matter of minutes. Hypoxia of the brain can be caused by cardiac arrest, respiratory failure or impaired local blood flow (ischemia), caused by the narrowing or complete obstruction of the blood vessel [2]. According to the World Health Organization, ischemic stroke of the brain is one of the main causes of death and disability of the human population around the world [3]. A number of biochemical markers were identified during the ischemic stroke that are primarily associated with imbalance in intracellular ionic composition, glutamate-mediated excitotoxicity [4–6], increased cytoplasmic Ca^{2+} level [7,8], mitochondrial dysfunction and decrease in ATP concentration [9,10], accumulation of succinate [11] and lactate [12], decrease in pH [12–14]. However, many details of pathological mechanisms are still poorly understood. It is believed that one of the key molecular mechanisms of stroke is oxidative stress caused by excessive production of reactive oxygen species in brain tissues after a restoration of blood flow (reperfusion). Several sources of ROS generation in stroke have been identified in cells, the NADPH-oxidase (NOXs) family and the mitochondrial respiratory chain being the main of them [11,15–18]. At present, there is still no consensus about which of these systems makes the main contribution to the development of oxidative stress in stroke. In this regard, several therapeutic targets have been proposed, including various types of NOXs proteins, in particular NOX1 [19], NOX2 [20–23], NOX4 [24,25], NOX5 [26], complexes of mitochondrial electron transport chain [11,27]. It is noteworthy that oxidative stress in damaged brain tissue during ischemia has always been determined indirectly by markers and characteristic metabolic abnormalities, while the real dynamics of ROS has never been recorded *in vivo*.

Various *in vitro* and *in vivo* experimental models have been developed to study the pathogenesis of stroke, as well as to develop therapeutic approaches. Neuronal cultures or cultured brain slices are widely used for *in vitro* research [28–31]. Several techniques have been developed to simulate ischemic cerebral stroke in mammals, mainly rodents [32,33]. The occlusion model of the middle cerebral artery (MCAO) is especially popular due to its ability to closely reproduce conditions of real stroke [34–37]. Traditionally, biochemical assays, morphological analysis and electrophysiological studies are used to monitor changes in cellular parameters in the brain during pathogenesis. The past decades have witnessed the advent of new technical solutions for biomedical research, including such powerful functional brain imaging techniques as magnetic resonance imaging (MRI) and positron emission tomography (PET). For example, for PET, the distribution of tracers labeled with positron-emitting isotopes allows identifying changes in the cerebral blood flow and variations in metabolism parameters, such as glucose utilization [38]. Optical methods, which help visualize structural and biochemical changes in brain cells with a high temporal and spatial resolution, make an enormous contribution to neurobiological research [39–46]. Despite the remarkable potential of the available arsenal of modern research approaches, their ability to study the real-time dynamics of many biochemical processes, especially those involving redox transformations, is still limited.

Genetically encoded fluorescent probes offer unique possibilities to study molecular processes in living systems of different scale and complexity. In this work, we utilize a fiber-optic interface technology in

combination with a palette of genetically encoded metabolic sensors to investigate the dynamics of pH and H_2O_2 *in vivo* during brain ischemia/reperfusion from the first seconds of pathogenesis. Moreover, to evaluate the utility of the cellular I/R models we present a detailed quantitative comparison of the results obtained for the living brain with those for cultured neurons *in vitro*.

2. Materials and methods

2.1. Genetic constructs and viruses

In the present work, we used adeno-associated viruses (AAVs) serotype 9 (AAV9). For a targeted expression of the necessary constructs in neurons, we used neuron-specific promoter – a constitutive hybrid promoter composed of the CMV immediate-early enhancer fused to human synapsin 1 promoter (hSyn1) [47]. hSyn1 promoter was inserted into the multiple cloning site (MCS) using *MluI* and *EcoRI* (FD, ThermoFisher Scientific) restriction sites of AAV9 plasmid (Stratagene). Genes encoding biosensors HyPer7 [48], SypHer3s [49] and SoNar [50] were inserted into the MCS using *EcoRI* and *HindIII* (FD, ThermoFisher Scientific) restriction sites of the AAV9-hSyn vector. To localize the biosensors in the mitochondrial matrix, the respective genes were equipped with a duplicated mitochondrial targeting sequence (MTS2) [51], while the “-cyto” constructs that did not contain subcellular localization signals were used for expression of biosensors in the cytosol. pC1-SypHer3s-dMito and pC1-HyPer7-dMito vectors with mitochondrial versions of biosensors were previously generated in our laboratory, in that work these genes were cloned into the AAV9-hSyn1 vector using *EcoRI* and *HindIII* (FD, ThermoFisher Scientific) restriction sites.

Minipreps and maxipreps were prepared using commercial kits according to the manufacturer's instructions (QIAPrep Spin Miniprep Kit, Qiagen). In order to study the functionality of the constructs, Hela Kyoto cells and primary neuronal cell culture were transfected with 1 μg plasmid DNA using FuGENE® HD (Promega) and Lipofectamine LTX with Plus Reagent (Invitrogen, ThermoFisher Scientific) respectively. Transfections were performed according to the manufacturer's protocols. Expression was analyzed 24 h (Hela Kyoto) and 1 week (primary neuronal cell culture) post-transfection under a fluorescent microscope (Zeiss Axiovert 200 M). The AAV9 particles bearing SoNar, SypHer3s and SypHer3s-dMito under the control of hSyn1 promoter were produced by Viral Core Facility (VCF) of the Charité – Universitätsmedizin Berlin. The AAV9 particles bearing HyPer7 and HyPer7-dMito under the control of hSyn1 promoter were produced by Viral Core Facility of IBCH. The virus titers were $1,81\text{E}+13$ VG/ml for AAV9-hSyn1-SypHer3s-cyto, $6,91\text{E}+12$ VG/ml for AAV9-hSyn1-SypHer3s-mito, $2,1\text{E}+11$ VG/ml for AAV9-hSyn1-SoNar-cyto, $1,4\text{E}+13$ VG/ml for AAV9-hSyn1-HyPer7-mito, and $4,7\text{E}+12$ VG/ml for AAV9-hSyn1-HyPer7-cyto.

2.2. Cell cultures

The mixed mouse primary embryonic hippocampal neuronal cell culture was obtained as described previously [52]. These cells were cultured in Minimal Essential Medium (MEM, Sigma), containing penicillin/streptomycin (1%, Gibco), Fetal Bovine Serum (FBS, 5%, BioloT), HEPES (10 mM, PanEko), D-Glucose (0,6%, Helicon), Sodium Bicarbonate (2 g/L, Dia-M), GlutaMax (1%, Gibco) and B27 supplement (2%, Gibco) at 37 °C in 5% CO_2 and seeded on 35 mm glass coverslips, which were treated with 0,1 mg/ml Poly-D-Lysine. For transient expression of biosensors, we used AAV-based vectors with cloned HyPer7, SypHer3s or SoNar genes. Cells were infected with viral particles at an MOI of 10

000 VG/cell.

2.3. Acute hypoxia/reoxygenation imaging on cultured neurons

To perform imaging of neurons in a state of hypoxia/reoxygenation, we used a Nikon Eclipse Ti2 inverted fluorescence microscope. For HyPer7, SypHer3s, SoNar excitation LED-DA/FI/TR/Cy5-B (DAPI/FITC/TRICTC/Cy5- Full Multiband Quad filters were used (ex = 352–404 nm, 461–488 nm), alongside with LED-DA/FI/TR/Cy5-B (DAPI/FITC/TRICTC/Cy5- Full Multiband Quad filters for emission (Em = 500–530 nm). Most of measurements were carried out using a 20X (S PLAN FL LWD 20x/0.70) and 40X (Plan Apo λ 40x/0.95 ∞ /0.11–0.23, WD 0.25–0.17 mm) objectives.

Before starting imaging experiments, the growth medium was changed to a KRS solution (120 mM NaCl, 5 mM KCl, 2 mM CaCl₂, 1 mM MgCl₂, 25 mM NaHCO₃, 5.5 mM HEPES, 10 mM D-glucose, pH 7.4), containing no serum, then cells were incubated at 37 °C in 5% CO₂ for 20 min.

The effect of acute hypoxia/reoxygenation on cultured neurons was investigated using a perfusion chamber. The cell dish was placed in the stage top incubator (Miniature Incubator TC-MWP, Bioscience Tools). Two 1L bottles with KRS solution were used for perfusion. The deoxygenated solution was prepared by bubbling 95% N₂/5% CO₂ gas mixture through the solution, the control solution was bubbled with 95% air/5% CO₂ (gas mixtures were produced by CO₂-O₂ controller CO₂-O₂-MI, Bioscience Tools, and CO₂ controller Tokai Hit). The solutions were supplied into the cell dish via tygon tubes by peristaltic pumps. The atmosphere in the incubator was 95% N₂/5% CO₂ under hypoxic conditions, 95% air/5% CO₂ under control and re-oxygenation conditions.

The oxygen content of the solutions was monitored using a multi-channel oximeter (Multi-Channel Oxygen Meter OXY-4 SMA (G3), PreSens Precision Sensing GmbH) connected to optical fibers recording the signal from a fluorescent oxygen sensors FTC-Pst3; PreSens Measurement Studio 2 software was used for data acquisition. Oxygen sensors were installed in both source bottles and inside the perfusion chamber – one in the deoxygenated solution inlet and one in the outlet tubes. With this setup we were able to induce hypoxia/reoxygenation in neurons in course of seconds and control the absence of oxygen directly in the cell dish.

The protocol of the experiment was as follows. First, the baseline fluorescence was recorded under control conditions for 15–20 min: a control solution was fed to the cell dish, the perfusion chamber was filled with 95% air/5% CO₂. Then fluorescence under hypoxia conditions was recorded for 35 min: deoxygenated solution was fed into the chamber; the perfusion chamber was filled with 95% N₂/5% CO₂. Then fluorescence was recorded under reperfusion conditions (same as in the control) for 15–20 min. At the end of the experiment, perfusion was stopped and H₂O₂ (200 μ M) or L-Lactate (20 mM) was added into the dish to record the maximal ratiometric response of the biosensors.

2.4. Animal husbandry

SHR rats purchased from Charles River laboratories, Germany, were used as founders whose offspring was used in the experiments. The animals were bred and housed in the animal facilities of the Institute of Bioorganic Chemistry of the Russian Academy of Sciences (IBCh RAS) and Pirogov Russian National Research Medical University in a 12 h light-dark cycle with free access to food and water. The work was accomplished under the supervision of the IBCh IACUC and following the Regulations of the Ministry of Health of the Russian Federation. All procedures were approved by IBCh IACUC protocol No.237.

2.5. Injection of viral particles and implantation of optical fiber probes into the rat brain

The animals of both sexes not heavier than 280 g were used in experiments. The rats were anesthetized with 2% isoflurane using SomnoSuite low-flow anesthesia system (Kent Scientific, USA). The head of the anesthetized animal was fixed in a stereotaxic frame, 0.25% bupivacaine was injected subcutaneously under the incision site. After skin incision all the transparent pericranial tissues were scraped away and the skull bones surface was thoroughly dried. Two small burr holes (0.4 mm) were made through the skull using a motorized drill under stereotaxic guidance (digital stereotaxic instrument, Stoelting Co) 0.9 mm posterior to bregma and 4.0 mm bilateral to midline. 33-gauge needle was slowly introduced into each burr hole on the depth of 5.2 mm below the surface of the skull and 1 μ l of AAV9 suspension was slowly injected into caudata nuclei using a 5- μ l Hamilton syringe connected to a stereotaxic injector (Stoelting Co). After the end of injections, implantable fiber probes (described below in the Methods section) were slowly inserted into each hole using a stereotaxic manipulator and ceramic ferrules were fixed on the skull with light-cured dental composite resin (DentLight-Flow A3, Vladmiva). The bone anchor screw was inserted into an additional 1-mm hole drilled in the posterior part of the skull. Then the ferrules and the screw were secured together by acrylic dental cement (Stoelting Co). After the end of the surgery the rat was injected with ketoprofen (5 mg/kg c.s.).

2.6. Stroke surgery – MCAO model

Stroke surgery was performed 3–4 weeks after fiber-probe implantation. The rats were anesthetized with 2% isoflurane using SomnoSuite low-flow anesthesia system (Kent Scientific, USA). The outer parts of the implanted fiber probes were cleaned with hydrogen peroxide and isopropyl alcohol, then a small drop of immersion oil was added to their tips. Then the ceramic ferrules were connected to a patch cable by a standard ceramic sleeve and additionally isolated from light with black tape. The transient 60-min occlusion of the middle cerebral artery followed by reperfusion was performed as described elsewhere [34] with minor modifications. Silicone-coated MCAO sutures (Doccol corporation) with a 0.5-cm tip length and 0.35–0.37-mm tip diameter were used for occlusion. The 0.25% bupivacaine was applied topically on the wound. After the end of the surgery the rat was injected with ketoprofen (5 mg/kg c.s.).

Animals from the sham group underwent the same surgical procedures, including the clamping of their left carotid artery, the only difference being that the filament in this group of animals was adjusted in such a way as to not reach the middle cerebral artery, thus causing no ischemia.

After 24 h of reperfusion, the animal was euthanized by an overdose of isoflurane followed by cervical dislocation, and decapitated. The brain was sliced into 2-mm coronal sections. The brain sections were immersed in a 1% solution of 2,3,5-triphenyltetrazolium chloride (TTC) in saline for 15–20 min. The infarct area was identified by the absence of red staining.

2.7. In vivo time-resolved, site-specific fiber-optic photometry with SypHer3s and HyPer7 sensors in rat brain tissues during the development of ischemic stroke

Dynamics of intracellular pH and H₂O₂ in rat brain structures was recorded in our experiments all-optically using implantable fiber-optic probes designed to serve the purposes of *in vivo* studies of an ischemic stroke in rats. In many of its aspects, the design of these fiber-optic probes builds upon the ideas and recipes developed earlier in fiber-optic neurointerface technologies [53–56]. However, *in vivo* site-specific studies of intracellular pH and H₂O₂ dynamics in rat's brain during an ischemic stroke impose a whole set of new requirements that

are specific to this type of studies and that need to be addressed via new solutions and approaches in the design of implantable fiber-optic probes. Specifically, the necessity to record pH and H₂O₂ dynamics simultaneously at several sites across rat's brain during a stroke is addressed in this study by implanting two fibers into rat's brain, with each of these fibers accurately positioned inside rat's brain to interrogate a specific, well-defined area inside rat's brain. Moreover, because the pH and H₂O₂ concentration are measured in this study via the ratio of fluorescence readouts from genetically encoded fluorescence sensors at two different wavelengths [49,57], each of the fiber probes implanted into rat's brain is designed to support two spectrally separated signal-delivery, signal-analysis, and signal-detection channels.

Two light emitting diodes (LEDs) with central wavelengths of 405 and 490 nm (M405F1 and M490F, Thorlabs) were used in our experiments to provide optical excitation for genetically encoded fluorescence sensors SypHer3s and HyPer7. The LED outputs were delivered via fiber-optic cables and collimated with 10.9-mm-focal-length fiber-optic collimators (Thorlabs, F220SMA-A). Suitable spectral filters were inserted in both arms of this scheme for a better spectral isolation of two radiation fields used for fluorescence-sensor excitation. The beams were then combined by a dichroic mirror (DM). A slightly tilted bandpass filter (ET480/20, Chroma) was used for this purpose and 490 nm light filtering. 405 nm light was filtered by a shortpass filter (FESH450, Thorlabs). The combined beam was focused with a 150-mm-focal-length lens and a microscope objective (10x, Olympus) to be coupled into long, ≈1.5-m segments of optical fiber (FG105UCA, Thorlabs). For the duration of measurements, these fiber segments were connected to the fiber probes implanted in rat's brain, thus providing an optical excitation of SypHer3s and HyPer7 fluorescence sensors at preselected sites within rat's brain. The fluorescence signal from these sensors is collected by the fiber probes implanted into rat's brain to be delivered to the detection system via the same fiber-optic tract, but in the opposite direction. Before reaching a CCD camera (4070C-GE-TE, Thorlabs), the fluorescence readout passes through an additional bandpass filter (Chroma, 525/50), which rejects the scattered excitation light, thus providing a high contrast of fluorescence readout detection. To ensure that the main contribution to the total fluorescence readout is the sensor fluorescence and not the autofluorescence background, which tends to vary from one rat to another, the signal collected by the fiber probe is redirected, with a flip mirror and polarization beam splitter, into another arm of the detection system, where it is analyzed with a home-built spectrometer.

We used glass-clad multimode fibers with 105/125 core/cladding diameter (FG105UCA, Thorlabs). The ≈1.5-m stretch of optical fiber was cut and fed through furcation tubing. Both fiber ends were stripped from acrylate coating and cleaved. The distal end was then coated with a UV-cured optical adhesive (NOA61, Thorlabs) and inserted inside a standard telecommunication ceramic ferrule for LC connectors. The glue was cured under UV illumination, then the protruding fiber tip was cleaved using a manual ruby cleaver and removed. After that ceramic ferrule was fixed inside polishing puck and manually polished using series of polishing sheets. Finally, a 5-cm piece of adhesive heat shrink tubing was passed over the ferrule and furcation tube, and shrunk using a heat gun. The proximate ends of two long fibers were glued together using a drop of NOA61 ≈3 cm from the tip and cleaved. This resulted in two nearly flat fiber tips located in the same focal plane.

Implantable fiber probes were fabricated on an in-house-built fiber-processing bench using in-house-tailored fiber components and fiber-processing tools. As the first step of the fabrication procedure, a factory-polished multimode patch cable was connected to a ceramic ferrule with a standard Lucent-connector-type ceramic sleeve. A short segment of bare optical fiber was then inserted inside the ceramic ferrule and fixed using a drop of UV-cured glue at the base of the ferrule. The length of each bare-fiber segment was chosen in such a way as to provide optical interrogation of a specific targeted area inside rat's brain. To this end, the length of each bare-fiber segment was adjusted with an accuracy well within 20 μm using a fiber cleaver (Thorlabs, XL411) driven by

a computer-controlled motorized translation stage (Thorlabs, MT1/M-Z8) on an in-house-assembled fiber-cleavage frame. Transmission properties of each fiber probe were carefully characterized, using a power meter (PM100D with an S120VC power sensor, Thorlabs). Only fiber probes with an overall transmission above 85% were used for implantation and subsequent measurements.

Time-resolved traces of the SypHer3s and HyPer7 fluorescence readout are recorded with a CCD camera, whose strobe output is read out with a multifunction I/O Device (I/O card, NI USB-6356), programmed with in-house-developed dedicated software, to gate the LED output (Fig. 1) within gating pulses of adjustable pulse width and repetition rate. With up to four fiber-probe endfaces simultaneously imaged onto the CCD camera via a suitably adjusted 4f imaging system, including a microscope objective (Olympus, 10X MPLN) and a 150-mm-focal-length lens (Fig. 1), each camera frame recorded at a given instant of time *t* yielded four fluorescence readouts from four specific sites inside rat's brain. Three frames were recorded for each *t*. Two of these frames captured fluorescence readouts from SypHer3s or HyPer7 as quantifiers of, respectively, pH or H₂O₂ at two excitation wavelengths (405 and 490 nm) from multiple sites within rat's brain (the inset in Fig. 1). The third frame records the overall background signal needed for accurate quantitative data analysis. The average power of LEDs was kept below 1 μW, which excluded any photobleaching within the entire time span (up to 3–4 h) needed to record full traces of 405- and 490-nm-light-driven fluorescence readouts from all the fiber probes used in a given measurement for a meaningful characterization of pH and H₂O₂ dynamics.

2.8. SypHer3s expression and purification

E. coli XL1 Blue cells were transformed with the pQE30 vector bearing SypHer3s genes with N-terminal His-tag. The protocol included an incubation of electrocompetent bacterial cells (40 μL) with a 1 μL of 50 ng/μL vector DNA on ice for 5 min. After this, the cells were transferred to the Gene Pulser/MicroPulser electroporation cuvettes (Bio-Rad), which were previously kept at −20 °C for 20 min, and subjected to the electroporation procedure according to the Ec1 program (MicroPulser, Bio-Rad). The transformed bacterial biomass was next incubated in 1 ml SOB at 37 °C and 650 rpm (Thermo-Shaker, Biosan) for 1 h to let the cells recover from the shock. At the next step, the suspension was distributed to bacterial plates with LB-agar medium containing 100 μg/ml ampicillin and the plates were kept at 37 °C for 15 h. As fluorescent proteins need time for their folding and chromophore maturation, which proceeds better at low temperatures, the bacteria were additionally incubated at 17 °C for 24 h to increase the yield of the functional biosensor. The average number of bacterial plates for a single protein purification procedure was 20. The bacterial colonies were washed from plates with cold PBS (137 mM NaCl, 2.7 mM KCl, 10 mM Na₂HPO₄, 1.8 mM KH₂PO₄, pH = 7.4) and the total volume of the sample was adjusted to 25 ml with the same buffer. To destroy cells, the suspension was sonicated in an ice bath (Sonic Vibra cell) according to the following program: 5 s/10 s sound/pause cycle with total sound duration of 8 min and amplitude of 32% (1/2" probe, 1/8" tapered microtip). The obtained lysates were centrifuged (Centrifuge 5424 R, Eppendorf) at 21 000 g and 4 °C for 30 min to precipitate insoluble fractions. To purify the biosensors, the supernatant was applied to a column filled with 4 ml of TALON Metal Affinity resin (Takara), previously equilibrated with cold PBS. The column was next washed with 40 ml of cold PBS to eliminate nonspecific components and after that step the target proteins were eluted by addition of 10 ml 250 mM imidazole solution in cold PBS. The obtained samples were next applied to a 10 ml Sephadex G-25 column (GE Healthcare) equilibrated with cold PBS to purify the proteins from imidazole. The protein concentration in the final sample was established with the use of Bicinchoninic Acid Kit (Sigma-Aldrich) and a 96-well plate analyzer (Tecan Infinite 200 PRO) according to the official protocol. The protein was stored at 4 °C and were used in *in vitro* studies

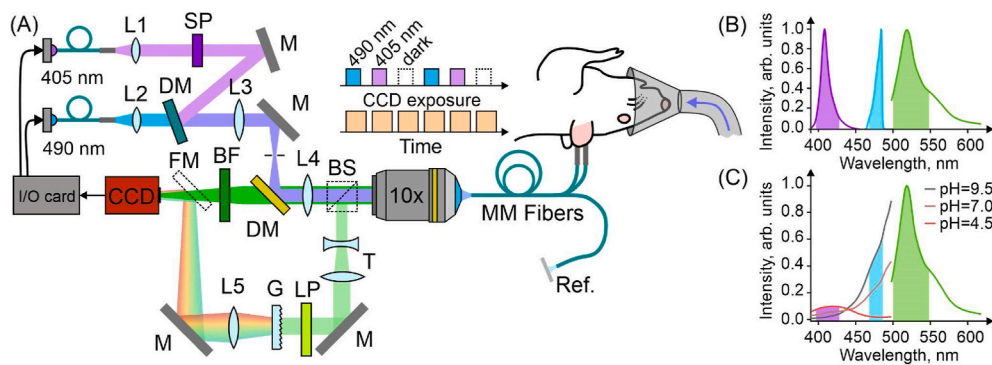


Fig. 1. Two-channel fiber-optic photometry for ratiometric pH and H_2O_2 sensing. (A) Optical setup: dielectric mirrors (M); dichroic mirrors (DM); multifunction I/O Device (I/O card); scientific-grade camera (CCD); bandpass filter (BF); shortpass filter (SP); microscope objective lens (10x); long multimode fibers (MM Fibers). A diagram of time-resolved wavelength-division fluorescence readout is shown in the inset. (B) Excitation light spectra of two LED sources (purple, 405 nm and cyan, 490 nm) and biosensors emission (green). (C) Excitation and emission spectra of SyPer3s at different pH. (For interpretation of the references to colour in this figure legend, the reader is referred to the Web version of this

article.)

within one day after purification.

2.9. Calibration of SyPer3s signal

For a quantitative analysis of intracellular pH based on the fluorescence readout from genetically encoded fluorescence sensor SyPer3s, this readout was carefully calibrated in a well-controlled experimental setting. In these experiments, the long section of the fiber probe was connected to its shorter, implantable counterpart, which was fixed on a micrometric stage. The tip of the implantable fiber probe was immersed into a cuvette containing pure buffer solution at room temperature and background signals were measured for both excitation wavelengths, 405 and 490 nm. The row of pH standards has the following composition: pH = 5.0 (Na_2HPO_4 – 0.64 mM, KH_2PO_4 – 66.02 mM); pH = 5.5 (Na_2HPO_4 – 2.60 mM, KH_2PO_4 – 64.06 mM); pH = 6.0 (Na_2HPO_4 – 8.07 mM, KH_2PO_4 – 58.59 mM); pH = 6.5 (Na_2HPO_4 – 20.87 mM, KH_2PO_4 – 45.80 mM); pH = 7.0 (Na_2HPO_4 – 40.81 mM, KH_2PO_4 – 25.86 mM); pH = 7.5 (Na_2HPO_4 – 56.82 mM, KH_2PO_4 – 9.87 mM); pH = 8.0 ($\text{Na}_2\text{B}_4\text{O}_7$ – 27.93 mM, HCl – 44.14 mM); pH = 8.5 ($\text{Na}_2\text{B}_4\text{O}_7$ – 31.13 mM, HCl – 37.74 mM); pH = 9.0 ($\text{Na}_2\text{B}_4\text{O}_7$ – 42.80 mM, HCl – 14.40 mM); pH = 9.5 ($\text{Na}_2\text{B}_4\text{O}_7$ – 39.50 mM, NaOH – 21.00 mM); pH = 10.0 ($\text{Na}_2\text{B}_4\text{O}_7$ – 29.50 mM, NaOH – 41.00 mM); pH = 10.5 ($\text{Na}_2\text{B}_4\text{O}_7$ – 26.40 mM, NaOH – 47.20 mM); pH = 11.0 ($\text{Na}_2\text{B}_4\text{O}_7$ – 25.00 mM, NaOH – 50.00 mM). The fiber tip was then immersed into a purified SyPer3s solution ($C \approx 500$ nM) with a certain pH. For reliable calibration, the fluorescence signal was averaged over at least 60 s.

2.10. Ex vivo HyPer7 test in brain tissues

The animal with expression of HyPer7 was euthanized by an overdose of isoflurane followed by cervical dislocation, and decapitated. The brain was immediately isolated, sliced into coronal sections and placed in the Petri dish. The ratiometric fluorescent signal was recorded using the same parameters that were utilized in the *in vivo* experiments. Next, H_2O_2 solutions at final concentrations of 10 mM and 30 mM were added into the dish. As a result, a saturating concentration of H_2O_2 was achieved, at which the ratiometric change in the signal reached its maximum and did not change with subsequent additions.

3. Results

3.1. Hypoxia/reoxygenation-driven changes of the NAD^+/NADH ratio, pH and H_2O_2 concentration in cultured murine primary neurons

We have constructed an experimental setup to investigate the effect of hypoxia and subsequent reoxygenation on biochemical parameters in cultured primary mouse hippocampal neurons (Fig. 2A). This setting provides extremely fast, accurate and well-controlled changes in the

oxygen level in the cell dish. In each series of experiments the oxygen concentration in the cell medium abruptly (within several seconds) changed from $\text{pO}_2 \sim 150$ mmHg to $\text{pO}_2 < 5$ mmHg, the neurons were subjected to hypoxia for 35 min, and then reoxygenated. We studied the dynamics of several biochemical parameters of neurons under conditions of hypoxia/reoxygenation using genetically encoded fluorescent biosensors: SoNar for the NAD^+/NADH monitoring [50], SyPer3s for pH [49] and HyPer7 for H_2O_2 [48]. SoNar, SyPer3s and HyPer7 are ratiometric cpYFP-based fluorescent proteins exhibiting two excitation maxima at ~ 410 and ~ 490 nm and one emission peak at ~ 520 nm. The changes in the levels of measured metabolites are reflected in the fluorescent ratiometric signal (F_{490}/F_{410}). The ratiometric signal does not depend on a biosensor expression level and other variables.

In order to test our experimental setup, we first applied it to detect NAD^+/NADH ratio changes during hypoxia/reoxygenation, as this parameter was studied earlier [58,59] and we can expect reduction of the NAD pool under hypoxia and oxidation during the reperfusion phase. Ratiometric SoNar signal (F_{395}/F_{470}) began to gradually increase with the onset of hypoxia and reached its maximum value in about 20 min (Fig. 2B) reflecting the reduction of NAD^+ to NADH. Reoxygenation very quickly led to the oxidation of the NAD pool; however, according to the biosensor fluorescent signal, the NAD^+/NADH ratio in the cytosol of neurons did not reach its initial value. The intracellular NAD^+/NADH ratio can be affected by changing the pyruvate/lactate ratio in the cellular medium due to the activity of cellular monocarboxylate transporters and lactate dehydrogenase. We have shown that the sequential addition of pyruvate and lactate to the same system led to a very rapid oxidation and reduction of the NAD pool in neurons, respectively. The amplitude of signal changes was comparable to what we observed with those caused by hypoxia/reoxygenation (Fig. 2B). These experiments confirmed the accuracy and validity of our experimental setup.

In the next series of experiments, we studied hypoxia/reoxygenation-driven pH changes in the cytosol and mitochondria of the mouse hippocampal neurons using SyPer3s biosensor [49]. Under hypoxia, the development of acidosis immediately began both in the cytosol and in the mitochondrial matrix. It is noteworthy that the biosensor localized in the cytosol is characterized by a more significant change in the signal. After normalization of oxygen level pH returned to the initial value in both compartments (Fig. 2C).

It is generally accepted that ROS contribute to development of hypoxia/reoxygenation related pathologies [60]. Some studies suggest ROS formation during the hypoxia phase [61] whereas others demonstrate oxidative stress upon reoxygenation [62]. To study generation of H_2O_2 under hypoxia/deoxygenation, we used ultrasensitive, fast, and pH-stable biosensor HyPer7 [48]. Despite the high sensitivity of HyPer7 to H_2O_2 , we did not observe substantial changes in the fluorescent signal under conditions of hypoxia/reoxygenation (Fig. 2D). However, under closer scrutiny, we found that during hypoxia the biosensor turned to a

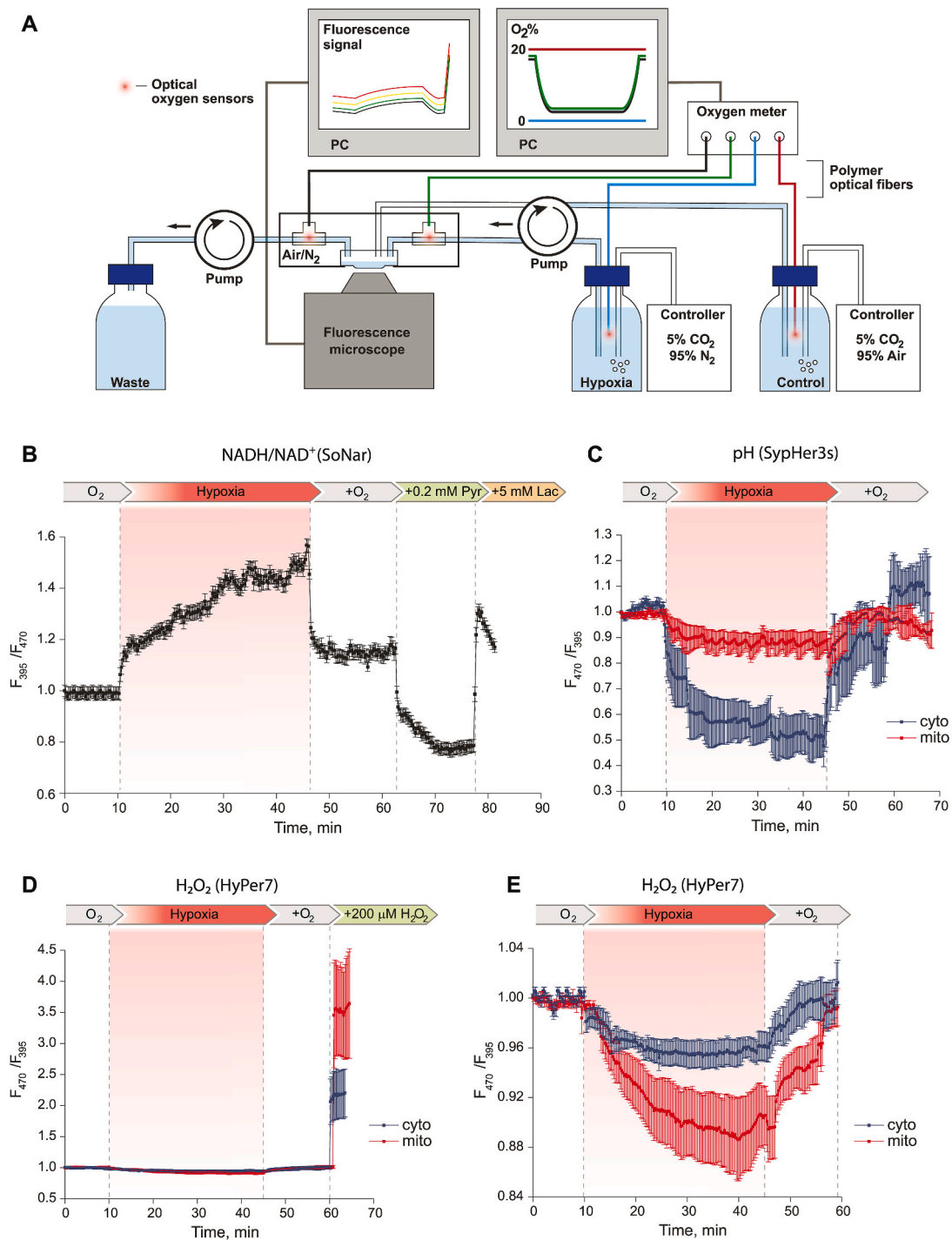


Fig. 2. Real-time detection of the NAD⁺/NADH ratio, pH and H₂O₂ concentration with genetically encoded fluorescent biosensors in the cytosol and mitochondrial matrix of cultured mouse primary hippocampal neurons during 35 min of hypoxia and subsequent reoxygenation. (A) Hypoxia/reoxygenation model setup. Under control and reoxygenation conditions, the control solution with normal oxygen concentration (pO₂ ~ 150 mmHg, maintained by gas controller and recorded by oxygen meter) was fed into the cell dish trough inlet tube without sensor, removed through outlet tube; perfusion chamber was supplied with air. Under hypoxic conditions, the deoxygenated solution with pO₂ < 5 mmHg of oxygen (maintained by gas controller and recorded by oxygen meter) was fed into the cell dish trough inlet tube with sensor, removed through outlet tube; perfusion chamber was supplied with nitrogen. Oxygen level in tanks and tubes, fluorescent signal from microscope were recorded in real-time mode. (B) The NAD⁺/NADH ratio dynamics during hypoxia/reoxygenation in neurons. Normalized signal of SoNar (ratio F_{395}/F_{470}) was averaged from 21 neurons in 2 experiments. A higher ratiometric signal of SoNar corresponds to a higher NADH/NAD⁺ ratio. (C) pH dynamics during hypoxia/reoxygenation in neurons. Normalized signal of SypHer3s (ratio F_{470}/F_{395}) was averaged from 184 neurons with mito-localization and 94 neurons with cyto-localization in 8 and 6 experiments, respectively. A higher ratiometric signal of SypHer3s corresponds to a more alkaline pH. (D) Dynamics of H₂O₂ concentration during hypoxia/reoxygenation in neurons against the background of exogenous H₂O₂ addition to determine the maximum response of HyPer7 biosensor in this system. Normalized signal of HyPer7 (ratio F_{470}/F_{395}) was averaged from 68 neurons with mito-localization of the biosensor and 120 neurons with cyto-localization in 4 experiments. A higher ratiometric signal of HyPer7 corresponds to a higher H₂O₂ concentration. (E) Dynamics of H₂O₂ concentration during hypoxia/reoxygenation in neurons. Normalized signal of HyPer7 (ratio F_{470}/F_{395}) was averaged from 203 neurons with mito-localization of the biosensor and 216 neurons with cyto-localization in 13 and 7 experiments, respectively. In all graphs error bars indicate standard error of mean.

more reduced state, which indicates a decrease in the basal concentration of H_2O_2 in comparison with normoxia (Fig. 2E). The decrease in H_2O_2 occurred gradually and the signal reached a stable value. Reoxygenation led to a faster change in the fluorescent signal of HyPer7 towards a more oxidized state. The signal of HyPer7 reached approximately its initial value before hypoxia. A similar dynamic was observed both in the cytosol and in the mitochondria of neurons. However, in the mitochondrial matrix the changes were more pronounced (Fig. 2E).

Thus, using our experimental approach we visualized in real time the dynamics of the redox state of the NAD pool and pH in cultured murine primary hippocampal neurons undergoing hypoxia/reoxygenation. However, under the same conditions, we did not register excessive ROS production but rather a slight decrease of H_2O_2 level during hypoxia phase.

3.2. *In vivo* studies of pH and H_2O_2 dynamics in rat brain tissues in ischemia/reperfusion model

The dynamics of biochemical processes in tissues *in vivo* can significantly differ from what is observed in cell cultures. For example, ischemic stroke is a complex pathological process involving different types of tissues and cells of an organism. To study ischemia/reperfusion-dependent pH and H_2O_2 dynamics in neurons of the brain *in vivo*, we performed transient middle cerebral artery occlusion (MCAO) on the SHR rats expressing genetically encoded pH indicator SypHer3s [49] and H_2O_2 indicator HyPer7 [48] bilaterally in the brain. SypHer3s was targeted to the cytosol, while HyPer7 was targeted to the mitochondrial matrix of neurons of the caudate nucleus. The choice of localizations was determined by our cell culture experiments: we have chosen the compartments with more pronounced changes in pH (cytosol) and H_2O_2 (matrix) in response to hypoxia/reoxygenation, thus reducing the number of animals in experiments. In addition, our experiments demonstrate that H_2O_2 produced in the cytosol quickly diffuses to the mitochondrial matrix, but the opposite direction of diffusion is restricted [48]. Therefore, HyPer7 targeted to the matrix would detect H_2O_2 regardless of the origin of the oxidant. Only one sensor per rat was used, so that both hemispheres of the same animal contained either SypHer3s or HyPer7 in the same cells and compartments. Caudate nucleus was chosen as a site for the virus injection as this structure is normally involved in ischemic injury caused by MCAO. In Fig. 3A and B, brain slices with expression of HyPer7-mito of a sham-operated rat and a rat with the ischemic stroke are demonstrated, with fluorescent region overlapping with the stroke area. The fluorescent signal was

simultaneously recorded in the healthy hemisphere in each experiment.

Dynamics of the fluorescent signal of biosensors *in vivo* in the rodent brain was studied by means of time-resolved photometry using fiber-optic probes implanted in rat's brain (Figs. 1 and 3C). The fluorescence of SypHer3s and HyPer7 in these experiments was driven by two LEDs emitting at 405 and 490 nm, as needed for ratiometric pH and H_2O_2 sensing. This approach allows one to drive and detect fluorescence in two channels through optical fibers implanted into the area of the rat brain containing the cells expressing the biosensor gene. Ratiometric measurements were performed in real time every 300 ms during the entire operation and for 2 h after the onset of ischemia. To avoid phototoxicity, an average pump output power inside rat's brain was kept below 0.7 μW , providing little or no photobleaching (less than 5% per hour).

The animals were anesthetized, and a silicone-coated suture was inserted intraluminally through the external carotid artery so that its tip blocked the origin of the middle cerebral artery (MCA). After 60 min of occlusion the suture was removed, ensuring the reperfusion of the ischemia area.

In order to convert the ratiometric signal of SypHer3s into specific pH value in the cells, before *in vivo* experiments we calibrated SypHer3s signal for the given setup using a purified protein preparation of the biosensor in buffer solutions with different pH values in the range 5.0–11.0. The signal was read through an optical fiber immersed in cuvettes with SypHer3s solutions (500 nM) in buffer systems. We used this calibration curve (Fig. 4A) in experiments on animals *in vivo* with intermediate values of pH being determined by cubic interpolation.

We found that MCAO leads to immediate and pronounced acidification in the ipsilateral hemisphere (Fig. 4). In several minutes, intracellular pH of the injured area dropped from 7.25 ± 0.08 (s.d.) to 6.7 ± 0.15 (s.d.). After reaching the minimum, pH started to rise slowly but steadily. The direction of the pH changes remained the same during the reperfusion phase, except transient but small increase during ischemia-to-reperfusion transition. The pH value did not reach its initial value neither during 1 h of reperfusion, nor, for most of the animals, 24 h later. Thus, ischemia/reperfusion induces strong and stable acidification of the ischemic core of stroke. pH in the hemisphere contralateral to MCAO did not show any pronounced dynamics, neither did pH in the brain of sham operated animals (Fig. 4).

We conducted a similar series of experiments with animals expressing HyPer7-mito to investigate the dynamics of H_2O_2 concentration in the mitochondrial matrix in rat brain neurons during the development of ischemia and subsequent reperfusion. To prove that the biosensor was not initially completely oxidized in the brain tissues of the animals as a

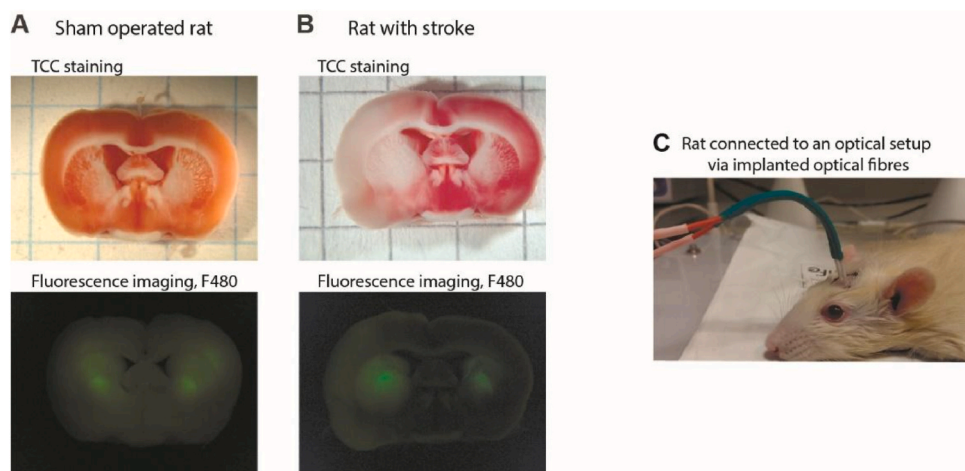


Fig. 3. Fiber-optic detection of the fluorescence readout from biosensors expressed in rat brain tissues. Brain slices of (A) sham operated rat and (B) rat with stroke (24h) exposed to the MCAO model. TTC staining was used to confirm ischemic injury. The presence of a fluorescent label (in the presented example, HyPer7-mito) was confirmed using fluorescence microscopy. (C) Photo of an animal with optical fibers implanted in the brain and connected to the optical cable of the setup.

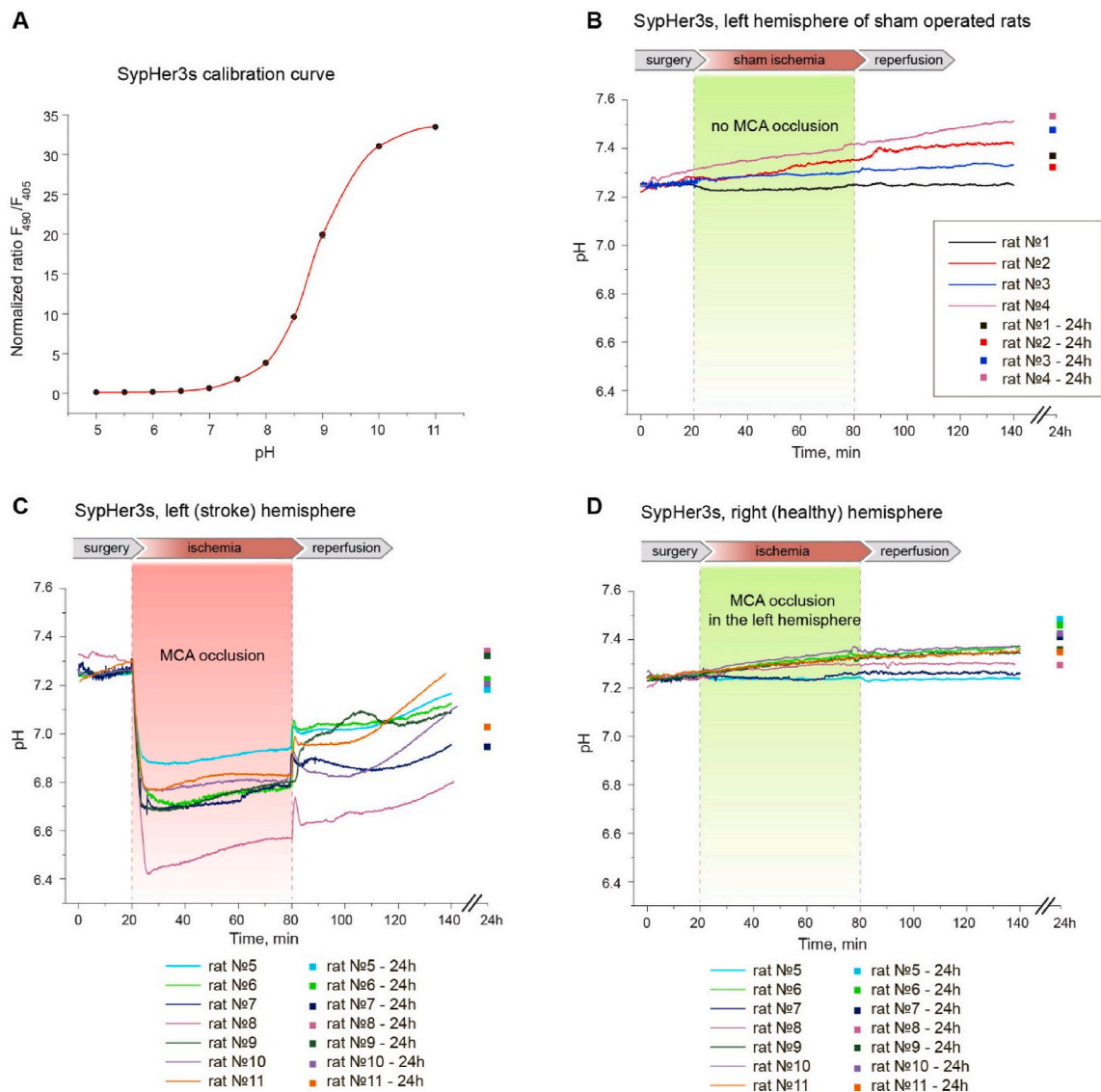


Fig. 4. *In vivo* time-resolved studies of pH dynamics in rat brain tissues during the development of ischemic stroke (MCAO model). Viral particles AAV9 with SypHer3s gene were injected into caudata nuclei of both hemispheres. (A) Calibration curve of the dependence of SypHer3s signal on the pH value obtained on purified protein preparation *in vitro*. Curve plotted from at least 3 measurements on purified protein. Error bars indicate standard deviation. (B) Dynamics of SypHer3s in the left hemisphere of sham operated rats. The animals of this group underwent all surgical procedures, except that the filament deliberately did not reach the MCA and did not cause occlusion. (C,D) Signal registration of SypHer3s with the setup was carried out through implanted fibers simultaneously at two points of the brain, corresponding the stroke zone in the left hemisphere (C) and healthy tissue in the right hemisphere (D). Each graph (B–C) reflects the pH dynamics in an individual rat. The dynamics of the signal was recorded continuously during the surgical procedures, the acute phase of the development of ischemic stroke (1 h ischemia + 1 h reperfusion); in addition, the signal value was measured the next day (separate points on the graphs).

result of the local inflammation caused by the injection of viral particles and implantation of optical fibers, we conducted preliminary measurements on freshly isolated brain tissue in response to exogenous H_2O_2 . Fig. 5A clearly demonstrates changes in HyPer7-mito fluorescent signal in tissues in response to stepwise H_2O_2 additions until the moment of complete saturation. The maximum response amplitude is ~ 2.5 -fold. Thus, in this system, the biosensor has a potential for oxidation and can be used to visualize oxidative stress.

During ischemia/reperfusion, we observed changes in the HyPer7-mito signal. Both ischemia and early phase of reperfusion induced slight increases in H_2O_2 that likely do not critically contribute to the development of the pathology. We registered a pronounced change in HyPer7-mito signal in the damaged area on the next day in all animals (Fig. 5C). The signal increased more than twofold, which corresponds to almost the maximum oxidation of the biosensor, according to the H_2O_2 saturation experiments (Fig. 5A). Thus, oxidative stress does occur, but

not in the acute phase of ischemic stroke.

On the next day after ischemia-reperfusion the animals were anesthetized by isoflurane and sacrificed. Subsequent TTC staining confirmed strokes in the MCAO hemispheres and the absence of infarcts in the contralateral hemispheres of all animals in the experimental groups, and no infarcts in both hemispheres of sham-operated animals.

4. Discussion

In the first part of the work, we studied how the dynamics of the $NAD^+/NADH$ ratio, pH value and H_2O_2 concentration change under hypoxia/reoxygenation conditions in the culture of primary hippocampal neurons using biosensors SoNar [50], SypHer3s [49] and HyPer7 [48], respectively. In our experiment, we carefully controlled the duration of hypoxia (35 min for cell culture experiments), followed by reoxygenation. We have demonstrated that the NAD pool reduction

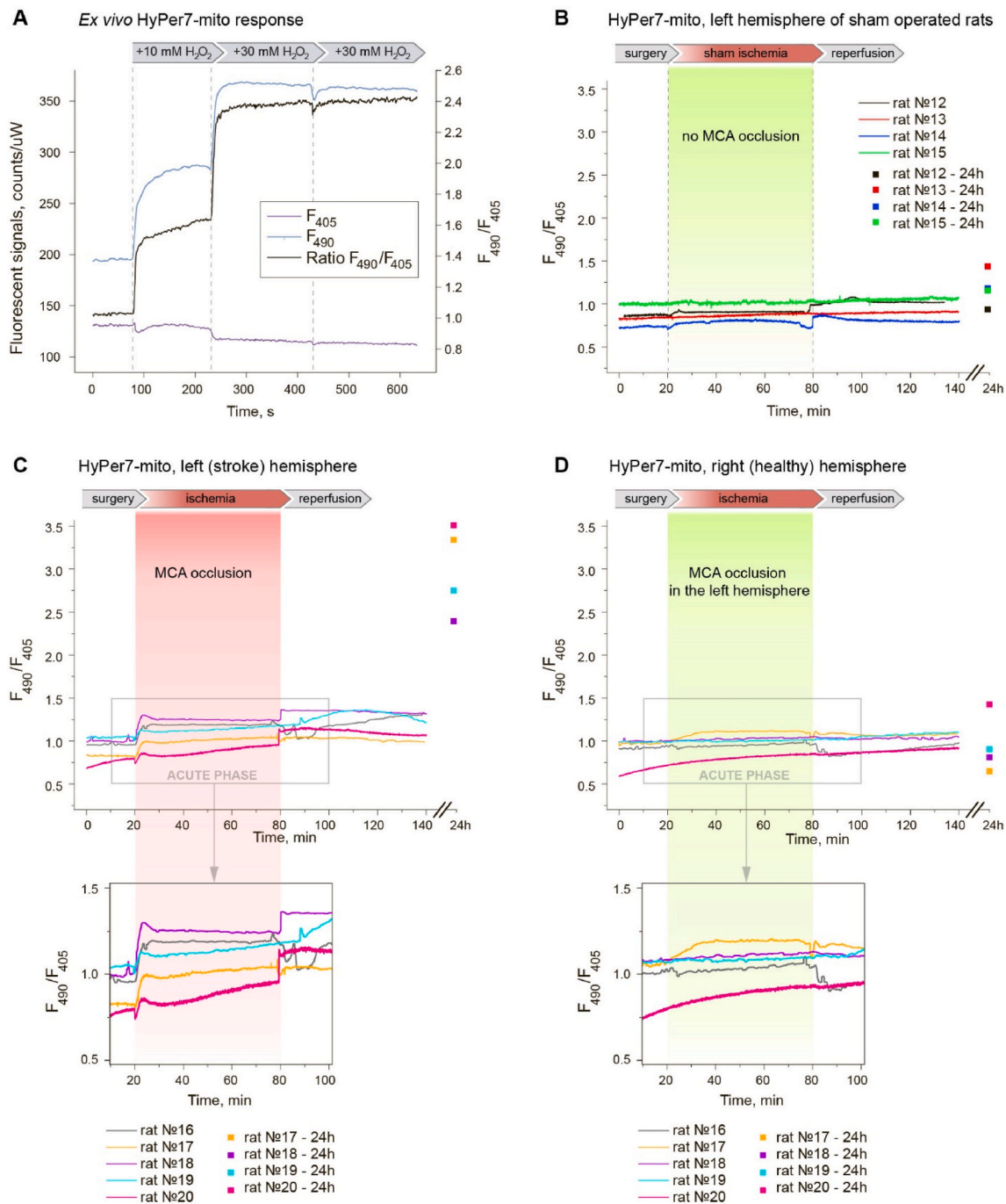


Fig. 5. *In vivo* time-resolved studies of H_2O_2 dynamics in rat brain tissues during the development of ischemic stroke (MCAO model). Viral particles AAV9 with HyPer7-mito gene were injected into caudata nuclei of both hemispheres. (A) *Ex vivo* HyPer7-mito response to exogenous H_2O_2 additions. (B) Dynamics of HyPer7-mito in the left hemisphere of sham operated rats. The animals of this group underwent all surgical procedures, except that the filament deliberately did not reach the MCA and did not cause occlusion. (C,D) Signal registration of HyPer7-mito with the setup was carried out through implanted fibers simultaneously at two points of the brain, corresponding the stroke zone in the left hemisphere (C) and healthy tissue in the right hemisphere (D). Each graph (B–C) reflects the H_2O_2 dynamics in an individual rat. The dynamics of the signal was recorded continuously during the surgical procedures, the acute phase of the development of ischemic stroke (1 h ischemia + 1 h reperfusion); in addition, the signal value was measured the next day (separate points on the graphs).

and pH decrease occur in neurons from the first seconds of the onset of hypoxia. It is noteworthy that we observed more pronounced changes in pH in the cytosol of neurons in comparison with the mitochondrial matrix. In conditions of a lack of oxygen, cells switch to anaerobic glycolysis, which occurs in the cytosol. As a result of this process, lactate accumulates and H^+ is generated as a result of ATP hydrolysis [63], which has been repeatedly confirmed by experimental data [64,65]. Thus, the global acidification of neurons caused by hypoxia, apparently,

begins in the cytosol, which is reflected in the dynamics of SypHer3s biosensor in our experiments. After reperfusion, the $NAD^+/NADH$ ratio and pH returned almost to the initial values. Under the same conditions, we registered the dynamics of H_2O_2 using an ultrasensitive biosensor HyPer7 [48]. However, we did not detect bursts of ROS generation in these cells. We recorded only a slight decrease in HyPer7 signal during hypoxia, which indicates decrease in the basal H_2O_2 level in the cells. After reoxygenation, the signal quickly returned to the initial value in

both studied compartments. This indicates that endogenous H₂O₂ production in this experimental system is limited by some yet unknown factor, likely the availability of substrates or the respiratory chain capacity, and the basal level of the oxidant could be, in fact, already maximal for the neurons.

It must be pointed out, however, that data obtained in the cell culture experiments may differ significantly from the real picture of the processes taking place *in vivo*. In particular, the pO₂ for cell cultures (in our case, ~150 mmHg) is unattainable in the living tissues where this parameter rarely exceeds 40 mmHg, and artifactual redox changes associated with the analysis of isolated biological samples is a well-known phenomenon (see, for example, [66]). In order to obtain more physiologically-relevant results we investigated the dynamics of pH and H₂O₂ concentration *in vivo* in neurons located in the central zone of ischemic stroke. For this, SypHer3s-cyto and HyPer7-mito sensors were expressed in the rat's caudate neurons. Using the standard procedure of transient MCAO, we induced unilateral cerebral ischemia and recorded continuously the dynamics of the studied parameters in both hemispheres during both ischemia and reperfusion.

We detected the development of powerful acidosis in the core zone of ischemic stroke. During the first few minutes after the onset of ischemia, the pH dropped by about 0.5 units (from pH 7.25 to pH 6.7). An important difference in the behavior of the pH dynamics *in vivo* during ischemic stroke from the previously observed pH changes in cultured neurons during hypoxia/reoxygenation was that the pH in the brain tissues in the ischemic core remained low for much longer after reperfusion.

Registration of pH changes in brain tissues during acidosis of tissues has already been carried out earlier using various approaches. For example, synthetic fluorescent pH probes have previously been used, some of them were suitable for spatio-temporal signal resolution in superficial brain tissues of anesthetized animals [67,68]. Many of the limitations associated with the disadvantages of pH-imaging using synthetic dyes have been overcome with the advent of positron emission tomography (PET) and magnetic resonance imaging (MRI) [69–73]. However, our approach used in this work to study the dynamics of biochemical events in the brains of laboratory animals *in vivo* provides a great flexibility of experimental design. Biosensors, which have a protein nature and are therefore encoded by the gene, can be easily targeted to any cell types of interest (neurons, astrocytes, microglia, etc.) and their organelles. The optical setup allows targeting any part of the brain or several areas at the same time by means of implanted optical fibers.

At the same time, while different research approaches exist to register pH in brain tissues, there were no direct methods for registering the development of oxidative stress. To the best of our knowledge, this work is the first example of direct intracellular H₂O₂ measurement in the brain tissues during ischemic stroke onset and development. HyPer7 localized in the mitochondria of neurons showed a slight increase in H₂O₂ concentration after the onset of hypoxia, which contradicts the generally accepted idea of significant post-ischemic ROS production [62]. We were also able to detect small step of H₂O₂ increase at the moment of reperfusion, but the pronounced changes in the signal of HyPer7 in the damaged area of the brain were detected only on the next day, which indicates either a delayed production of ROS in the ischemic stroke, or total metabolic failure of the tissue resulting in an inability of thio-redoxin system to maintain HyPer7 in the reduced state. Both the shapes and directions of H₂O₂ changes differed between the cell culture and *in vivo* models demonstrating poor correlation between these systems.

Another possibility is that oxidative stress during brain ischemia/reperfusion occurs not via hydrogen peroxide production, but via lipid peroxidation. In this case the radical chain reaction spreads in the cellular membrane, and lipid peroxides cannot be detected by HyPer7. Indeed, lipid peroxidation is known to be associated with the ischemia/reperfusion injury [74].

It is also possible that the production of ROS coincides with the development of the inflammatory process caused by the activation of

microglia and infiltration of neutrophils. In subsequent experiments, we aim to investigate the roles of various types of cells and tissues in the pathogenesis of stroke. In particular, it would be important to record the biosensor signal for a longer time, taking the animals out of anesthesia, in order to find the exact moment of the H₂O₂ generation onset.

Author disclosure statement

No competing financial interests exist.

Acknowledgements

Supported by the Russian Science Foundation (RSF) Grant 17-15-01175 (to D.S.B.); by the Ministry of Science and Higher Education, grant 075-15-2019-1933 and 14.Z50.31.0040; Russian Foundation for Basic Research, projects 18-29-20031 and 19-02-00473; Russian Science Foundation, project 20-12-00088 – ultrabroadband optical science; and the Welch Foundation, grant A-1801-20180324.

References

- [1] P. Mergenthaler, U. Lindauer, G.A. Dienel, A. Meisel, Sugar for the brain: the role of glucose in physiological and pathological brain function, *Trends Neurosci.* 36 (2013) 587–597, <https://doi.org/10.1016/j.tins.2013.07.001>.
- [2] D. Kuriakose, Z. Xiao, Pathophysiology and treatment of stroke: present status and future perspectives, *Int. J. Mol. Sci.* 21 (2020), <https://doi.org/10.3390/ijms21207609>.
- [3] W. Johnson, O. Onuma, M. Owolabi, S. Sachdev, Stroke: a global response is needed, *Bull. World Health Organ.* 94 (2016), <https://doi.org/10.2471/BLT.16.181636>, 634–634A.
- [4] H. Benveniste, Glutamate, microdialysis, and cerebral ischemia: lost in translation? *Anesthesiology* 110 (2009) 422–425, <https://doi.org/10.1097/ALN.0b013e318194b620>.
- [5] T.W. Lai, S. Zhang, Y.T. Wang, Excitotoxicity and stroke: identifying novel targets for neuroprotection, *Prog. Neurobiol.* 115 (2014) 157–188, <https://doi.org/10.1016/j.pneurobio.2013.11.006>.
- [6] D. Belov Kirdajova, J. Kriska, J. Tureckova, M. Anderova, Ischemia-triggered glutamate excitotoxicity from the perspective of glial cells, *Front. Cell. Neurosci.* 14 (2020) 51, <https://doi.org/10.3389/fncel.2020.00051>.
- [7] D. Bano, P. Nicotera, Ca²⁺ signals and neuronal death in brain ischemia, *Stroke* 38 (2007) 674–676, <https://doi.org/10.1161/01.STR.0000256294.46009.29>.
- [8] K. Szydłowska, M. Tymianski, Calcium, ischemia and excitotoxicity, *Cell Calcium* 47 (2010) 122–129, <https://doi.org/10.1016/j.ceca.2010.01.003>.
- [9] N.J. Solenski, C.G. diPierro, P.A. Trimmer, A.-L. Kwan, G.A. Helm, Ultrastructural changes of neuronal mitochondria after transient and permanent cerebral ischemia, *Stroke* 33 (2002) 816–824, <https://doi.org/10.1161/hs0302.104541>.
- [10] N.R. Sims, H. Muyderman, Mitochondria, oxidative metabolism and cell death in stroke, *Biochim. Biophys. Acta* (2010) 80–91, <https://doi.org/10.1016/j.bbdis.2009.09.003>, 1802.
- [11] E.T. Chouchani, V.R. Pell, E. Gaude, D. Akseintjević, S.Y. Sundier, E.L. Robb, A. Logan, S.M. Nadtochiy, E.N.J. Ord, A.C. Smith, F. Eyassu, R. Shirley, C.-H. Hu, A.J. Dare, A.M. James, S. Rogatti, R.C. Hartley, S. Eaton, A.S.H. Costa, P. S. Brookes, S.M. Davidson, M.R. Duchon, K. Saeb-Parsy, M.J. Shattock, A. J. Robinson, L.M. Work, C. Frezza, T. Krieg, M.P. Murphy, Ischaemic accumulation of succinate controls reperfusion injury through mitochondrial ROS, *Nature* 515 (2014) 431–435, <https://doi.org/10.1038/nature13909>.
- [12] S. Rehncrona, I. Rosén, B.K. Siesjö, Brain lactic acidosis and ischemic cell damage: 1. Biochemistry and neurophysiology, *J. Cerebr. Blood Flow Metabol.* 1 (1981) 297–311, <https://doi.org/10.1038/jcbfm.1981.34>.
- [13] M. Chopp, S. Frinak, D.R. Walton, M.B. Smith, K.M. Welch, Intracellular acidosis during and after cerebral ischemia: *in vivo* nuclear magnetic resonance study of hyperglycemia in cats, *Stroke* 18 (1987) 919–923, <https://doi.org/10.1161/01.str.18.5.919>.
- [14] K. Katsura, A. Ekholm, B. Asplund, B.K. Siesjö, Extracellular pH in the brain during ischemia: relationship to the severity of lactic acidosis, *J. Cerebr. Blood Flow Metabol.* 11 (1991) 597–599, <https://doi.org/10.1038/jcbfm.1991.109>.
- [15] S. Manzanero, T. Santro, T.V. Arumugam, Neuronal oxidative stress in acute ischemic stroke: sources and contribution to cell injury, *Neurochem. Int.* 62 (2013) 712–718, <https://doi.org/10.1016/j.neuint.2012.11.009>.
- [16] A. Patt, A.H. Harken, L.K. Burton, T.C. Rodell, D. Piermattei, W.J. Schorr, N. B. Parker, E.M. Berger, I.R. Horesch, L.S. Terada, Xanthine oxidase-derived hydrogen peroxide contributes to ischemia reperfusion-induced edema in gerbil brains, *J. Clin. Invest.* 81 (1988) 1556–1562, <https://doi.org/10.1172/JCI113488>.
- [17] E. Kumura, T. Yoshimine, K.I. Iwatsuki, K. Yamanaka, S. Tanaka, T. Hayakawa, T. Shiga, H. Kosaka, Generation of nitric oxide and superoxide during reperfusion after focal cerebral ischemia in rats, *Am. J. Physiol.* 270 (1996) C748–C752, <https://doi.org/10.1152/ajpcell.1996.270.3.C748>.
- [18] M. Kim, A. Stepanova, Z. Niatsetskaia, S. Sosunov, S. Arndt, M.P. Murphy, A. Galkin, V.S. Ten, Attenuation of oxidative damage by targeting mitochondrial

- complex I in neonatal hypoxic-ischemic brain injury, *Free Radic. Biol. Med.* 124 (2018) 517–524, <https://doi.org/10.1016/j.freeradbiomed.2018.06.040>.
- [19] D.-H. Choi, J.-H. Kim, K.-H. Lee, H.-Y. Kim, Y.-S. Kim, W.S. Choi, J. Lee, Role of neuronal NADPH oxidase 1 in the peri-infarct regions after stroke, *PLoS One* 10 (2015), e0116814, <https://doi.org/10.1371/journal.pone.0116814>.
- [20] T. Kahles, R.P. Brandes, Which NADPH oxidase isoform is relevant for ischemic stroke? The case for nox 2, *Antioxidants Redox Signal.* 18 (2013) 1400–1417, <https://doi.org/10.1089/ars.2012.4721>.
- [21] H. Chen, G.S. Kim, N. Okami, P. Narasimhan, P.H. Chan, NADPH oxidase is involved in post-ischemic brain inflammation, *Neurobiol. Dis.* 42 (2011) 341–348, <https://doi.org/10.1016/j.nbd.2011.01.027>.
- [22] X.N. Tang, Z. Zheng, R.G. Giffard, M.A. Yenari, Significance of marrow-derived nicotinamide adenine dinucleotide phosphate oxidase in experimental ischemic stroke, *Ann. Neurol.* 70 (2011) 606–615, <https://doi.org/10.1002/ana.22476>.
- [23] T.M. De Silva, V.H. Brait, G.R. Drummond, C.G. Sobey, A.A. Miller, Nox2 oxidase activity accounts for the oxidative stress and vasomotor dysfunction in mouse cerebral arteries following ischemic stroke, *PLoS One* 6 (2011), e28393, <https://doi.org/10.1371/journal.pone.0028393>.
- [24] C. Kleinschnitz, H. Grund, K. Wingle, M.E. Armitage, E. Jones, M. Mittal, D. Barit, T. Schwarz, C. Geis, P. Kraft, K. Barthel, M.K. Schuhmann, A.M. Herrmann, S. G. Meuth, G. Stoll, S. Meurer, A. Schrewe, L. Becker, V. Gailus-Durner, H. Fuchs, T. Klopstock, M.H. de Angelis, K. Jandeleit-Dahm, A.M. Shah, N. Weissmann, H.H. H.W. Schmidt, Post-stroke inhibition of induced NADPH oxidase type 4 prevents oxidative stress and neurodegeneration, *PLoS Biol.* 8 (2010), <https://doi.org/10.1371/journal.pbio.1000479>.
- [25] A.I. Casas, E. Geuss, P.W.M. Kleikers, S. Mencil, A.M. Herrmann, I. Buendia, J. Egea, S.G. Meuth, M.G. Lopez, C. Kleinschnitz, H.H.H.W. Schmidt, NOX4-dependent neuronal autotoxicity and BBB breakdown explain the superior sensitivity of the brain to ischemic damage, *Proc. Natl. Acad. Sci. U. S. A.* 114 (2017) 12315–12320, <https://doi.org/10.1073/pnas.1705034114>.
- [26] A.I. Casas, P.W. Kleikers, E. Geuss, F. Langhauser, T. Adler, D.H. Busch, V. Gailus-Durner, M.H. de Angelis, J. Egea, M.G. Lopez, C. Kleinschnitz, H.H. Schmidt, Calcium-dependent blood-brain barrier breakdown by NOX5 limits postreperfusion benefit in stroke, *J. Clin. Invest.* 129 (2019) 1772–1778, <https://doi.org/10.1172/JCI124283>.
- [27] Z.V. Niatsetskaia, S.A. Sosunov, D. Matsiukevich, I.V. Utkina-Sosunova, V. I. Ratner, A.A. Starkov, V.S. Ten, The oxygen free radicals originating from mitochondrial complex I contribute to oxidative brain injury following hypoxia-ischemia in neonatal mice, *J. Neurosci.* 32 (2012) 3235–3244, <https://doi.org/10.1523/JNEUROSCI.6303-11.2012>.
- [28] Q. Li, X. Han, J. Wang, Organotypic hippocampal slices as models for stroke and traumatic brain injury, *Mol. Neurobiol.* 53 (2016) 4226–4237, <https://doi.org/10.1007/s12035-015-9362-4>.
- [29] P.M. Holloway, F.N.E. Gavins, Modeling ischemic stroke in vitro: status quo and future perspectives, *Stroke* 47 (2016) 561–569, <https://doi.org/10.1161/STROKEAHA.115.011932>.
- [30] W.Q. Dong, A. Schurr, K.H. Reid, C.B. Shields, C.A. West, The rat hippocampal slice preparation as an in vitro model of ischemia, *Stroke* 19 (1988) 498–502, <https://doi.org/10.1161/01.str.19.4.498>.
- [31] M.J.P. Richard, T.M. Saleh, B. El Bahh, J.A. Zidichouski, A novel method for inducing focal ischemia in vitro, *J. Neurosci. Methods* 190 (2010) 20–27, <https://doi.org/10.1016/j.jneumeth.2010.04.017>.
- [32] J.B. Casals, N.C.G. Pieri, M.L.T. Feitosa, A.C.M. Ercolin, K.C.S. Roballo, R.S. N. Barreto, F.F. Bressan, D.S. Martins, M.A. Miglino, C.E. Ambrósio, The use of animal models for stroke research: a review, *Comp. Med.* 61 (2011) 305–313.
- [33] F. Fluri, M.K. Schuhmann, C. Kleinschnitz, Animal models of ischemic stroke and their application in clinical research, *Drug Des. Dev. Ther.* 9 (2015) 3445–3454, <https://doi.org/10.2147/DDDT.S56071>.
- [34] M. Rupadevi, S. Parasuraman, R. Raveendran, Protocol for middle cerebral artery occlusion by an intraluminal suture method, *J. Pharmacol. Pharmacother.* 2 (2011) 36–39, <https://doi.org/10.4103/0976-500X.77113>.
- [35] K. Uluç, A. Miranpuri, G.C. Kujoth, E. Aktüre, M.K. Başkaya, Focal cerebral ischemia model by endovascular suture occlusion of the middle cerebral artery in the rat, <https://doi.org/10.3791/1978>, 2011.
- [36] E.Z. Longa, P.R. Weinstein, S. Carlson, R. Cummins, Reversible middle cerebral artery occlusion without craniectomy in rats, *Stroke* 20 (1989) 84–91, <https://doi.org/10.1161/01.str.20.1.84>.
- [37] T. Chiang, R.O. Messing, W.-H. Chou, Mouse model of middle cerebral artery occlusion, <https://doi.org/10.3791/2761>, 2011.
- [38] P.J. Magistretti, I. Allaman, A cellular perspective on brain energy metabolism and functional imaging, *Neuron* 86 (2015) 883–901, <https://doi.org/10.1016/j.neuron.2015.03.035>.
- [39] F. Tian, K. Deguchi, T. Yamashita, Y. Ohta, N. Morimoto, J. Shang, X. Zhang, N. Liu, Y. Ikeda, T. Matsuura, K. Abe, In vivo imaging of autophagy in a mouse stroke model, *Autophagy* 6 (2010) 1107–1114, <https://doi.org/10.4161/auto.6.8.13427>.
- [40] J.W. Taraska, W.N. Zagotta, Fluorescence applications in molecular neurobiology, *Neuron* 66 (2010) 170–189, <https://doi.org/10.1016/j.neuron.2010.02.002>.
- [41] R. Ni, M. Vaas, W. Ren, J. Klohs, Noninvasive detection of acute cerebral hypoxia and subsequent matrix-metalloproteinase activity in a mouse model of cerebral ischemia using multispectral-optoacoustic tomography, *Neurophotonics* 5 (2018), 015005, <https://doi.org/10.1117/1.NPh.5.1.015005>.
- [42] L.M. Palmer, G.J. Stuart, Membrane potential changes in dendritic spines during action potentials and synaptic input, *J. Neurosci.* 29 (2009) 6897–6903, <https://doi.org/10.1523/JNEUROSCI.5847-08.2009>.
- [43] C. Stosiek, O. Garaschuk, K. Holthoff, A. Konnerth, In vivo two-photon calcium imaging of neuronal networks, *Proc. Natl. Acad. Sci. U. S. A.* 100 (2003) 7319–7324, <https://doi.org/10.1073/pnas.1232232100>.
- [44] S. Witte, A. Negrean, J.C. Lodder, C.P.J. de Kock, G. Testa Silva, H.D. Mansvelder, M. Louise Groot, Label-free live brain imaging and targeted patching with third-harmonic generation microscopy, *Proc. Natl. Acad. Sci. U. S. A.* 108 (2011) 5970–5975, <https://doi.org/10.1073/pnas.1018743108>.
- [45] B.A. Flusberg, A. Nimmerjahn, E.D. Cocker, E.A. Mukamel, R.P.J. Barretto, T.H. Ko, L.D. Burns, J.C. Jung, M.J. Schnitzer, High-speed, miniaturized fluorescence microscopy in freely moving mice, *Nat. Methods* 5 (2008) 935–938, <https://doi.org/10.1038/nmeth.1256>.
- [46] A. de Groot, B.J. van den Boom, R.M. van Genderen, J. Coppens, J. van Veldhuijzen, J. Bos, H. Hoedemaker, M. Negrello, I. Willuhn, C.I. De Zeeuw, T. M. Hoogland, NiNScope, a versatile miniscope for multi-region circuit investigations, *Elife* 9 (2020), <https://doi.org/10.7554/eLife.49987>.
- [47] S. Kügler, E. Kilic, M. Bähr, Human synapsin 1 gene promoter confers highly neuron-specific long-term transgene expression from an adenoviral vector in the adult rat brain depending on the transduced area, *Gene Ther.* 10 (2003) 337–347, <https://doi.org/10.1038/sj.gt.3301905>.
- [48] V.V. Pak, D. Ezerija, O.G. Lyublinskaya, B. Pedre, P.A. Tyurin-Kuzmin, N. M. Mishina, M. Thauvin, D. Young, K. Wahni, S.A. Martínez Gache, A. D. Demidovich, Y.G. Ermakova, Y.D. Maslova, A.G. Shokhina, E. Eroglu, D.S. Bilan, I. Bogeski, T. Michel, S. Vriz, J. Messens, V.V. Belousov, Ultrasensitive genetically encoded indicator for hydrogen peroxide identifies roles for the oxidant in cell migration and mitochondrial function, *Cell Metabol.* 31 (2020) 642–653, <https://doi.org/10.1016/j.cmet.2020.02.003>, e6.
- [49] Y.G. Ermakova, V.V. Pak, Y.A. Bogdanova, A.A. Kotlobay, I.V. Yampolsky, A. G. Shokhina, A.S. Panova, R.A. Marygina, D.B. Staroverov, D.S. Bilan, H. Sies, V. V. Belousov, SypHer3s: a genetically encoded fluorescent ratiometric probe with enhanced brightness and an improved dynamic range, *Chem. Commun.* 54 (2018) 2898–2901, <https://doi.org/10.1039/c8cc08740c>.
- [50] Y. Zhao, Q. Hu, F. Cheng, N. Su, A. Wang, Y. Zou, H. Hu, X. Chen, H.-M. Zhou, X. Huang, K. Yang, Q. Zhu, X. Wang, J. Yi, L. Zhu, X. Qian, L. Chen, Y. Tang, J. Loscalzo, Y. Yang, SoNar, a highly responsive NAD⁺/NADH sensor, allows high-throughput metabolic screening of anti-tumor agents, *Cell Metabol.* 21 (2015) 777–789, <https://doi.org/10.1016/j.cmet.2015.04.009>.
- [51] R. Rizzuto, H. Nakase, B. Darras, A. Francke, G.M. Fabrizi, T. Mengel, F. Walsh, B. Kadenbach, S. Dimauro, E. Schon, A gene specifying subunit VIII of human cytochrome c oxidase is localized to chromosome 11 and is expressed in both muscle and non-muscle tissues, *J. Biol. Chem.* 264 18 (1989) 10595–10600.
- [52] M. Seibenhener, L. Wooten M.L., Isolation and culture of hippocampal neurons from prenatal mice, *J. Vis. Exp.* 65 (2012) e3634, <https://doi.org/10.3791/3634>.
- [53] M.R. Warden, J.A. Cardin, K. Deisseroth, Optical neural interfaces, *Annu. Rev. Biomed. Eng.* 16 (2014) 103–129, <https://doi.org/10.1146/annurev-bioeng-071813-104733>.
- [54] L.V. Doronina-Amitonova, I.V. Fedotov, O.I. Ivashkina, M.A. Zots, A.B. Fedotov, K. V. Anokhin, A.M. Zheltikov, Implantable fiber-optic interface for parallel multisite long-term optical dynamic brain interrogation in freely moving mice, *Sci. Rep.* 3 (2013) 3265, <https://doi.org/10.1038/srep03265>.
- [55] C.K. Kim, S.J. Yang, N. Pichamoorthy, N.P. Young, I. Kauvar, J.H. Jennings, T. N. Lerner, A. Berndt, S.Y. Lee, C. Ramakrishnan, T.J. Davidson, M. Inoue, H. Bito, K. Deisseroth, Simultaneous fast measurement of circuit dynamics at multiple sites across the mammalian brain, *Nat. Methods* 13 (2016) 325–328, <https://doi.org/10.1038/nmeth.3770>.
- [56] Y. Sych, M. Chernysheva, L.T. Sumanovski, F. Helmchen, High-density multi-fiber photometry for studying large-scale brain circuit dynamics, *Nat. Methods* 16 (2019) 553–560, <https://doi.org/10.1038/s41592-019-0400-4>.
- [57] A.A. Lanin, A.S. Chebotarev, M.S. Pochechuev, I.V. Kelmanson, D.A. Kotova, D. S. Bilan, Y.G. Ermakova, A.B. Fedotov, A.A. Ivanov, V.V. Belousov, A.M. Zheltikov, Two- and three-photon absorption cross-section characterization for high-brightness, cell-specific multiphoton fluorescence brain imaging, *J. Biophot.* 13 (2020), e201900243, <https://doi.org/10.1002/jbio.201900243>.
- [58] O. Garofalo, D.W. Cox, H.S. Bachelard, Brain levels of NADH and NAD⁺ under hypoxic and hypoglycaemic conditions in vitro, *J. Neurochem.* 51 (1988) 172–176, <https://doi.org/10.1111/j.1471-4159.1988.tb04851.x>.
- [59] A. Mayevsky, Brain NADH redox state monitored in vivo by fiber optic surface fluorometry, *Brain Res. Rev.* 7 (1984) 49–68, [https://doi.org/10.1016/0165-0173\(84\)90029-8](https://doi.org/10.1016/0165-0173(84)90029-8).
- [60] C. Li, R.M. Jackson, Reactive species mechanisms of cellular hypoxia-reoxygenation injury, *Am. J. Physiol. Cell Physiol.* 282 (2002) C227–C241, <https://doi.org/10.1152/ajpcell.00112.2001>.
- [61] R. Chen, U.H. Lai, L. Zhu, A. Singh, M. Ahmed, N.R. Forsyth, Reactive oxygen species formation in the brain at different oxygen levels: the role of hypoxia inducible factors, *Front. Cell Dev. Biol.* 6 (2018) 132, <https://doi.org/10.3389/fcell.2018.00132>.
- [62] D.N. Granger, P.R. Kvietys, Reperfusion injury and reactive oxygen species: the evolution of a concept, *Redox Biol.* 6 (2015) 524–551, <https://doi.org/10.1016/j.redox.2015.08.020>.
- [63] P.W. Hochachka, T.P. Mommsen, Protons and anaerobiosis, *Science* 219 (1983) 1391–1397, <https://doi.org/10.1126/science.6298937>.
- [64] W. Paschen, B. Djuricic, G. Mies, R. Schmidt-Kastner, F. Linn, Lactate and pH in the brain: association and dissociation in different pathophysiological states, *J. Neurochem.* 48 (1987) 154–159, <https://doi.org/10.1111/j.1471-4159.1987.tb13140.x>.
- [65] D.J. Combs, R.J. Dempsey, M. Maley, D. Donaldson, C. Smith, Relationship between plasma glucose, brain lactate, and intracellular pH during cerebral

- ischemia in gerbils, *Stroke* 21 (1990) 936–942, <https://doi.org/10.1161/01.str.21.6.936>.
- [66] M.S. Nanadikar, A.M.V. Leon, S. Borowik, A. Hillemann, A. Zieseniss, V. V. Belousov, I. Bogeski, P. Rehling, J. Dudek, D.M. Katschinski, O₂ affects mitochondrial functionality ex vivo, *Redox Biol* 22 (2019) 101152, <https://doi.org/10.1016/j.redox.2019.101152>.
- [67] X. Sun, Y. Wang, S. Chen, W. Luo, P. Li, Q. Luo, Simultaneous monitoring of intracellular pH changes and hemodynamic response during cortical spreading depression by fluorescence-corrected multimodal optical imaging, *Neuroimage* 57 (2011) 873–884, <https://doi.org/10.1016/j.neuroimage.2011.05.040>.
- [68] B. Bo, Y. Li, W. Li, Y. Wang, S. Tong, Optogenetic translocation of protons out of penumbral neurons is protective in a rodent model of focal cerebral ischemia, *Brain Stimul* 13 (2020) 881–890, <https://doi.org/10.1016/j.brs.2020.03.008>.
- [69] M. Senda, N.M. Alpert, B.C. Mackay, R.B. Buxton, J.A. Correia, S.B. Weise, R. H. Ackerman, D. Dorer, F.S. Buonanno, Evaluation of the ¹¹C₁₈O₂ positron emission tomographic method for measuring brain pH. II. Quantitative pH mapping in patients with ischemic cerebrovascular diseases, *J. Cerebr. Blood Flow Metabol.* 9 (1989) 859–873, <https://doi.org/10.1038/jcbfm.1989.120>.
- [70] K.E. Henry, A.M. Chaney, V.L. Nagle, H.C. Cropper, S. Mozaffari, G. Slaybaugh, K. Parang, O.A. Andreev, Y.K. Reshetnyak, M.L. James, J.S. Lewis, Demarcation of sepsis-induced peripheral and central acidosis with pH (low) insertion cycle peptide, *J. Nucl. Med.* 61 (2020) 1361–1368, <https://doi.org/10.2967/jnumed.119.233072>.
- [71] L. Yu, Y. Chen, M. Chen, X. Luo, S. Jiang, Y. Zhang, H. Chen, T. Gong, J. Zhou, C. Li, Amide proton transfer MRI signal as a surrogate biomarker of ischemic stroke recovery in patients with supportive treatment, *Front. Neurol.* 10 (2019) 104, <https://doi.org/10.3389/fneur.2019.00104>.
- [72] G.W.J. Harston, Y.K. Tee, N. Blockley, T.W. Okell, S. Thandeswaran, G. Shaya, F. Sheerin, M. Cellerini, S. Payne, P. Jezzard, M. Chappell, J. Kennedy, Identifying the ischaemic penumbra using pH-weighted magnetic resonance imaging, *Brain* 138 (2015) 36–42, <https://doi.org/10.1093/brain/awu374>.
- [73] J. Zhou, J.-F. Payen, D.A. Wilson, R.J. Traystman, P.C.M. van Zijl, Using the amide proton signals of intracellular proteins and peptides to detect pH effects in MRI, *Nat. Med.* 9 (2003) 1085–1090, <https://doi.org/10.1038/nm907>.
- [74] M. Serteser, T. Ozben, S. Gumuslu, S. Balkan, E. Balkan, Lipid peroxidation in rat brain during focal cerebral ischemia: prevention of malondialdehyde and lipid conjugated diene production by a novel antiepileptic, lamotrigine, *Neurotoxicology* 23 (2002) 111–119, [https://doi.org/10.1016/s0161-813x\(02\)00018-9](https://doi.org/10.1016/s0161-813x(02)00018-9).